Settling of finite-size particles in turbulence at different volume fractions

(Article begins on next page)

Settling of finite-size particles in turbulence at different volume fractions

Walter Fornari · Sagar Zade · Luca Brandt · Francesco Picano

Abstract We study the settling of finite-size rigid spheres in quiescent fluid and in sustained homogeneous isotropic turbulence (HIT) by direct numerical simulations using an immersed boundary method to account for the dispersed solid phase. We consider semi-dilute and dense suspensions of rigid spheres with solid volume fractions $\phi = 0.5\% - 10\%$, solid-to-fluid density ratio $R = 1.02$, and Galileo number (i.e. the ratio between buoyancy and viscous forces) $Ga = 145$. In HIT, the nominal Reynolds number based on the Taylor microscale is $Re_\lambda \simeq 90$, and the ratio between the particle diameter and the nominal Kolmogorov scale is $(2a)/\eta \simeq 12$ (being a the particle radius). We find that in HIT, the mean settling speed is less than that in quiescent fluid for all ϕ. For $\phi = 0.5\%$, the mean settling speed in HIT is 8% less than in quiescent fluid. However, by increasing the volume fraction the difference in mean settling speed between quiescent fluid and HIT cases reduces, being only 1.7% for $\phi = 10\%$. Indeed, while at low ϕ the settling speed is strongly altered by the interaction with turbulence, at large ϕ this is mainly determined by the (strong) hindering effect. This is similar in quiescent fluid and in HIT, leading to similar mean settling speeds. On the contrary, particle angular velocities are always found to increase with ϕ. These are enhanced by the interaction with turbulence, especially at low ϕ. In HIT, the correlations of particle lateral velocity fluctuations oscillate around zero before decorrelating completely. The time period of the oscillation seems proportional to the ratio between the integral length-scale of turbulence and the particle characteristic terminal velocity. Regarding the mean square particle displacement, we find

W. Fornari · S. Zade · L. Brandt
Linné Flow Centre and Swedish e-Science Research Centre (SeRC),
KTH Mechanics, SE-100 44 Stockholm, Sweden
E-mail: fornari@mech.kth.se

F. Picano
Department of Industrial Engineering, University of Padova,
Via Venezia 1, 35131 Padua, Italy

that it is strongly enhanced by turbulence in the direction perpendicular to gravity, even at the largest ϕ. Finally, we investigate the collision statistics for all cases and find the interesting result that the collision frequency is larger in quiescent fluid than in HIT for $\phi = 0.5\% - 1\%$. This is due to frequent drafting-kissing-tumbling events in quiescent fluid. The collision frequency becomes instead larger in HIT than in still fluid for $\phi = 5\% - 10\%$, due to the larger relative approaching velocities in HIT, and to the less intense drafting-kissing-tumbling events in quiescent fluid. The collision frequency also appears to be almost proportional to the estimate for small inertial particles uniformly distributed in space, though much smaller. Concerning the turbulence modulation, we find that the mean energy dissipation increases almost linearly with ϕ, leading to a large reduction of Re_λ.

1 Introduction

Sedimentation is a process commonly observed in a wide range of natural processes and industrial applications. Among these we recall for example fluidized beds, sedimentation basins and tanks for water treatment, volcanic eruptions and the formation of fluvial bedforms. Typically, these applications involve a large number of falling particles in either quiescent fluids or in already-turbulent flows. In both scenarios, the suspension dynamics depends on several parameters like the size and density of the particles (compared to the size of the container and the density of the fluid), their shape and deformability, and their concentration within the mixture. In addition, when the settling occurs in turbulence the dynamics is altered by the interaction between particles and turbulence eddies of sizes ranging from the largest, integral scale to the smallest dissipative, Kolmogorov scales. In such cases, additional parameters must be taken into account, like the ratio between the particle diameter and a characteristic lengthscale of the turbulence (e.g., either the integral or the Kolmogorov lengthscales), as well as the ratio of the particle relaxation time and a turbulence time scale, and the relative turbulence intensity (defined as the ratio between the root-mean-square turbulence velocity, and the particle terminal falling speed). Clearly, due to the very large number of parameters involved, sedimentation is a very rich phenomenon that is still far from being fully understood.

Concerning sedimentation in quiescent fluid, several works have investigated the importance of particle inertia, shape and volume fraction [38,32,2]. If we limit our attention to an isolated rigid spherical particle, then its dynamics depends on the solid-to-fluid density ratio, R, and the Galileo number (i.e. the ratio between buoyancy and viscous forces), Ga. For ellipsoidal particles the aspect ratio is another important parameter. Depending on these parameters, different settling regimes are observed [21,10,9,7,2]: e.g. steady vertical, oblique, time-periodic oscillating, zig-zagging, helical, and chaotic for a falling sphere (the intermediate regimes are different for non-spherical particles).

When it comes to suspensions of spherical particles, it is typically known that the mean settling speed $\langle V_{p,z} \rangle$ is a decreasing function of the volume fraction, ϕ, and is hence smaller than the terminal settling speed of an isolated particle, V_t [29,38]. This is due to the hindrance effect. Indeed, if we consider a batch sedimentation system, the mean velocity of the mixture must be zero. However, since particles are falling towards the bottom wall, the surrounding fluid is displaced and moves in the opposite direction, therefore hindering the settling. At low terminal Reynolds numbers ($Re_t \leq 10$, based on V_t), the reduction in $\langle V_{p,z} \rangle / V_t$ with ϕ is sufficiently well described by the empirical formula proposed by Richardson & Zaki [29]. For larger Reynolds numbers, Re_t, several authors proposed corrections to this formula [16,38]. However, the picture changes at Galileo numbers Ga larger than 155. Indeed, it was shown that at large Ga and moderate ϕ ($\sim 0.5\%$), particles tend to form fast settling clusters and, as a consequence, the mean settling speed $\langle V_{p,z} \rangle$ actually increases above V_t [32,39,20]. This peculiar behavior was shown to be related to the specific settling regime of isolated particles (i.e. steady oblique falling). More recently, Ardekani et al. [2] found that suspensions of oblate particles exhibit a similar collective behavior ($\langle V_{p,z} \rangle > V_t$, for $\phi \simeq 0.5\%$), at much smaller Galileo numbers ($Ga = 60$). For this type of particles, indeed, the phenomenon known as drafting-kissing-tumbling is modified with respect to what observed for spheres [15]. In particular, after the interacting particle-pair have been drafted and kissed, the tumbling phase is suppressed (at least for an isolated pair). Consequently, the two particles settle together for long times with a mean speed that is 1.5 times V_t [2]. Since these particles stick for long times and create long and intense wakes, more and more particles are entrained, and clusters of up to 5 particles can be formed. Due to the no-slip condition, the fluid surrounding these clusters is dragged and moves fastly along the gravity direction. Hence, more particles migrate to these downward-moving fluid region, and a columnar-like structure of particles is formed. Finally, at steady-state $\langle V_{p,z} \rangle \simeq 1.33 V_t$ [11].

Concerning the sedimentation in turbulence, most of previous investigations focused on particles smaller or at most comparable in size to the Kolmogorov lengthscale, η. In these conditions, turbulence can either enhance, reduce or inhibit the settling. For example, if we consider small inertial particles with $Re_t \ll 1$, then it is known that in turbulence these particles would accumulate at the peripheries of the vortices, where vorticity is low and strain-rate is high [30]. However, since these particles are settling, they are preferentially swept towards regions of downward-moving fluid. As a consequence of this *inertial bias* and *preferential sweeping*, the particles are accelerated by the downdrafts and they fast-track the turbulence eddies with an increased mean settling speed. This was first observed from simulations of point-particles settling in random flows [25], and in turbulence [34], and later confirmed by experiments [27,1,35,36].
For these small particles, the enhancement of the mean settling speed progressively vanishes as particle inertia increases [17]. Finally, when the Stokes terminal velocity ($2(R-1)ga^2/(9\nu)$), where g is gravity, a the particle radius

and ν the fluid viscosity) becomes larger than the turbulent velocity fluctuation intensity (u'), a reduction in mean settling speed is observed. Indeed, when the terminal settling speed is sufficiently high, the particles fall almost along straight vertical paths and are hence unable to side step the turbulent eddies. Fast-tracking is suppressed and particles end up mostly oversampling upward moving fluid. And, as suggested by Nielsen [27], falling particles need longer times to cross these regions (loitering). This behavior was observed both experimentally [26,27,35,22] and numerically [34,17]. However, to observe this in direct numerical simulations (DNS) it is necessary to employ nonlinear drag corrections that account for finite particle Reynolds numbers, as shown by Good et al. [17].

Less is known about the settling of finite-size particles in turbulent environments. Recently, Fornari et al. [13] studied the sedimentation of finite-size spherical particles in homogeneous isotropic turbulence (HIT) . In particular, they considered dilute suspensions of spheres with diameter of about twelve Kolmogorov scales, density ratio $R = 1.02$, and Galileo number $Ga = 145$, and compared the results with those for quiescent fluid. They found that in HIT the mean settling speed reduces by about 8% when compared with the same quantity in quiescent fluid. This reduction is attributed to unsteady phenomena arising from the turbulence-induced modification of the particle boundary layer, and to the quick disruption of the particle wakes by the turbulence (see also [3,19]).
Later on the same group investigated the importance of the Galileo number, Ga, on the settling in HIT [14]. Taking the above-mentioned case as reference, they considered 3 additional Ga of $19, 60$ and 200, while keeping fixed the nominal features of the turbulence (i.e., constant nominal u'). By varying Ga, the reference terminal velocity of isolated particles (V_t) changes, and so does the relative turbulence intensity, defined as u'/V_t. It was found that at large $Ga = 145, 200$, when $u'/V_t < 1$, the mean settling speed reduces by about 8% with respect to that in quiescent fluid. However, by decreasing Ga the reduction in mean settling speed increases, being around 55% for $Ga = 19$, when $u'/V_t > 1$. Higher the turbulence r.m.s. velocity, stronger the reduction in mean settling speed related to the enhancement of the nonlinear component of the drag acting on the particles. Notice that similar reductions in mean settling speed were observed experimentally by Byron [6] for Taylor-scale particles.

In the present study, we consider suspensions of finite-size rigid spheres settling in HIT. We fix the solid-to-fluid density ratio and the Galileo number to $R = 1.02$ and $Ga = 145$, and increase the solid volume fraction from $\phi = 0.5\%$ to 10% to assess its effect on the dynamics. The density ratio is close to that of aquatic organisms in water, with most animals' densities falling within 2-3% of the density of water [6]. Besides this direct implication, in our previous study, we found that at constant $Ga < 155$, varying the density ratio R in the range $(1; 1.5)$ lead to very similar results [14]. The background sustained homogeneous isotropic turbulent flow has a nominal Reynolds number based on the Taylor microscale Re_λ of about 90, while the ratio $(2a)/\eta$ is approximately 12. The settling in quiescent fluid is also studied, and results are compared

with those in HIT. The study is performed in HIT as it is assumed that rigid boundaries (both lateral and bottom walls) are far away from the test section. Considering a bottom wall would be prohibitive from a computational point of view. Indeed, an excessively long box would be needed to limit the influence of the vertical length on the statistics, and to have enough statistical samples. On the other hand, the presence of lateral walls would lead to nonuniform particle distributions and spatially dependent statistics. These interesting aspects are out of the scope of present work and will be considered in future studies.

From our study we found important and sometimes unexpected differences in the behaviors of semi-dilute versus dense suspensions when turbulent and quiescent environmental conditions are considered, e.g. settling speeds, rotation rates, dispersion. Interestingly, we found that the collision frequency is larger in quiescent fluid than in HIT for semi-dilute cases, i.e. $\phi = 0.5\% - 1\%$. We attribute this behavior to the fact that in quiescent environment at low ϕ, there is a high frequency of drafting-kissing-tumbling events between particle pairs. The probability to find a particle pair at contact is hence larger in quiescent fluid than in HIT and governs the collision kernel. The collision frequency becomes instead larger in HIT than in still fluid for dense cases, $\phi = 5\% - 10\%$, as the relative approaching velocity is slightly larger in HIT.

2 Set-up and Methodology

The sedimentation of finite-size spherical particles is studied in a computational domain with periodic boundary conditions in the x, y and z directions, with gravity acting in the positive z direction. The computational box has size $32a \times 32a \times 320a$, and we consider 4 volume fractions $\phi = [0.5, 1, 5, 10]\%$, corresponding to $391, 782, 3911$ and 7823 particles. The spheres are rigid, non-Brownian, and slightly heavier than the suspending fluid with density ratio $R = 1.02$. In addition to R and ϕ, the other parameter that governs the settling is the Galileo number

$$Ga = \frac{\sqrt{(R-1)\, g(2a)^3}}{\nu}. \tag{1}$$

This non-dimensional number quantifies the importance of the gravitational forces acting on the particle with respect to viscous forces, and in the present simulation is set to 145. With this combination of R and ϕ, an isolated sphere falls steadily along a straight vertical path and, when it comes to dilute suspensions, no clustering is observed [32,13]. In all cases, the particles are initially randomly distributed in the computational volume with zero velocity and rotation.

To generate and sustain an isotropic and homogeneous turbulent flow field, a random forcing is applied to the first wavenumber in the directions perpendicular to gravity, and to the tenth wavenumber in the settling direction. Since in the settling direction the box length is 10 times that in the other directions, forcing the tenth wavenumber is equivalent to forcing the first wavenumber in

$\eta/(2a)$	u'	k	$\lambda/(2a)$	Re_λ	ϵ	T_e	Re_{L_0}
0.084	0.30	0.13	1.56	90	0.0028	46.86	1205

Table 1 Turbulent flow parameters in particle units (namely, particle diameter $2a$ and the characteristic terminal velocity V_t of an isolated particle). Here k is the turbulent kinetic energy, λ is the Taylor microscale, $T_e = k/\epsilon$ is the eddy turnover time and Re_{L_0} is the Reynolds number based on the integral lengthscale $L_0 = k^{3/2}/\epsilon$.

a cube of size $32a \times 32a \times 32a$. This procedure has been successfully adopted in [32,13]. The forcing is δ-correlated in time and of fixed amplitude [33,40]. The unladen turbulent field is characterized by the Reynolds number based on the Taylor microscale, $Re_\lambda = \lambda u'/\nu$, where u' is the turbulence r.m.s. velocity, and $\lambda = \sqrt{15\nu u'^2/\epsilon}$ is the transverse Taylor length scale (being ϵ the energy dissipation). This is approximately 90 in our simulations. The ratio between the Kolmogorov lengthscale $\eta = (\nu^3/\epsilon)^{1/4}$ and the grid spacing $(\eta/\Delta x)$ is approximately 1.3 while the particle diameter is approximately 12η. Finally, the ratio between the turbulence r.m.s. velocity, u', and the characteristic terminal velocity, V_t, is approximately 0.3. The parameters of the turbulent flow field are summarized in table 1.

The simulations have been performed using an immersed boundary method that fully models the coupling between the solid and fluid phases [5]. The flow is evolved according to the incompressible Navier-Stokes equations

$$\nabla \cdot \mathbf{u}_f = 0 \tag{2}$$

$$\frac{\partial \mathbf{u}_f}{\partial t} + \mathbf{u}_f \cdot \nabla \mathbf{u}_f = -\frac{1}{\rho_f}\nabla p + \nu \nabla^2 \mathbf{u}_f + \mathbf{f} \tag{3}$$

where $\mathbf{u}_f$, ρ_f and ν are the fluid velocity, density and kinematic viscosity, respectively while p and $\mathbf{f}$ are the pressure and the force field used to maintain turbulence and model the presence of particles. Particle motion is instead governed by the Newton-Euler Lagrangian equations for the particle centroid linear and angular velocities

$$\rho_p V_p \frac{d\mathbf{u}_p}{dt} = \oint_{\partial \mathcal{V}_p} \boldsymbol{\tau} \cdot \mathbf{n} \, dS + (\rho_p - \rho_f) V_p \mathbf{g} \tag{4}$$

$$\frac{dI_p \boldsymbol{\omega}_p}{dt} = \oint_{\partial \mathcal{V}_p} \mathbf{r} \times \boldsymbol{\tau} \cdot \mathbf{n} \, dS \tag{5}$$

where ρ_p, V_p and I_p are the particle density, volume and moment of inertia; $\mathbf{g}$ is the gravitational acceleration; $\boldsymbol{\tau} = -p\mathbf{I} + 2\mu\mathbf{E}$ is the fluid stress, with $\mathbf{E} = \left(\nabla \mathbf{u}_f + \nabla \mathbf{u}_f^T\right)/2$ the deformation tensor; $\mathbf{r}$ is the distance vector from the center of the particle while $\mathbf{n}$ is the unity vector normal to the particle surface $\partial \mathcal{V}_p$. Dirichlet boundary conditions for the fluid phase are enforced on the particle surfaces as $\mathbf{u}_f|_{\partial \mathcal{V}_p} = \mathbf{u}_p + \boldsymbol{\omega}_p \times \mathbf{r}$.

By means of the immersed boundary method, the boundary condition at the moving fluid/solid interfaces is modelled by an additional force on the

right-hand side of the Navier-Stokes equations. This allows us to discretize the computational domain with a fixed staggered mesh on which the fluid phase is evolved using a second-order finite-difference scheme. Time integration is performed by a third-order Runge-Kutta scheme combined with pressure correction at each sub-step. When the distance between two particles becomes smaller than twice the mesh size, lubrication models based on Brenner's asymptotic solution [4] are used to correctly reproduce the interaction between the particles. In addition, a soft-sphere collision model is used to account for collisions between particles, and an almost elastic rebound is ensured with a restitution coefficient set at 0.97. A cubic mesh with eight points per particle radius is used for the results presented, which corresponds to $256 \times 256 \times 2560$ grid points. This resolution is a good compromise in terms of accuracy and computational cost as shown in previous publications [5, 23, 28, 24, 12, 13], wherein more details and validations of the numerical code are provided. Note finally that zero total volume flux is imposed in the simulations.

When studying settling in a turbulent flow, the fluid phase at rest is evolved for approximately six eddy turnover times with the δ-correlated forcing in order to reach a statistically steady regime of fully developed turbulence at $Re_\lambda \simeq 90$. It is possible that using a forcing that is not δ-correlated in time could lead to a minor modification of the results [33]. When the box shows the typical behavior of fully developed turbulence, the solid phase is added to the system. Then the statistics are collected after a transient phase so that the difference between the statistics presented here and those computed from half the samples is below 1% for the first and second moments. For the lower ϕ (0.5% and 1%), the transient is approximately 4 eddy turnover times ($T_e = k/\epsilon$) in HIT and at least 15 relaxation times ($\tau_p = 2Ra^2/(9\nu)$) in the quiescent cases. For the larger ϕ (5% and 10%), the transient is shorter and approximately 2 eddy turnover times (in HIT), and 7 relaxation times (in still fluid). Shorter transient time (or equivalently development lengths) have also been experimentally observed in pipe flow suspensions of neutrally buoyant particles [18]. After these transient periods, velocities and accelerations oscillate on average with a constant amplitude around the mean. In the following we will use $\mathbf{V}_f$ and $\mathbf{V}_p$ for the fluid and particle velocity.

3 Results

3.1 Particle statistics

One of the most interesting results of the present study is that in an already-turbulent flow, the mean settling speed $\langle V_{p,z} \rangle$ is smaller than in quiescent fluid. However, the reduction in $\langle V_{p,z} \rangle$ with respect to quiescent environments, decreases as the volume fraction ϕ increases. Here, the notation $\langle \cdot \rangle$ denotes averaging over the total number of particles and time (ensemble average).

The mean settling speed $\langle V_{p,z} \rangle$ normalized by V_t, is shown as a function of ϕ in figure 1(a) for both quiescent and turbulent cases. We see that at

a)   b)
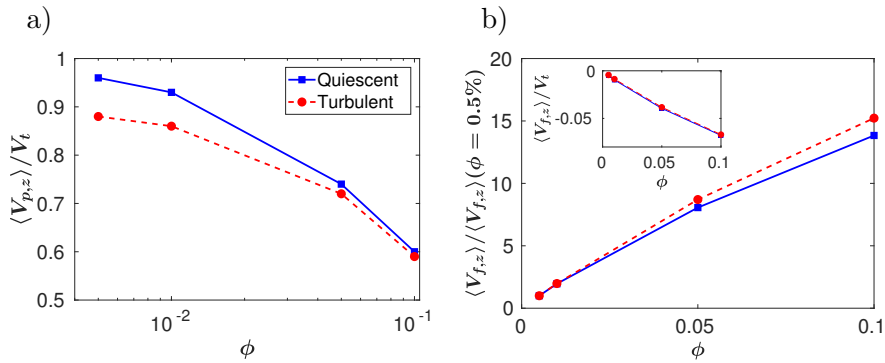
Fig. 1 (a) The mean settling speed, $\langle V_{p,z} \rangle$, normalized by V_t as function of the solid volume fraction ϕ, for both quiescent and turbulent cases. (b) The mean fluid speed in the direction of gravity, $\langle V_{f,z} \rangle$, normalized by the value for $\phi = 0.5\%$, in both quiescent and turbulent cases. The inset shows the actual values of $\langle V_{f,z} \rangle$ (normalized by V_t).

low $\phi = 0.5\%$, the mean settling speed is approximately 8.3% lower in HIT than in quiescent fluid. The change in $\langle V_{p,z} \rangle$ between HIT and quiescent fluid decreases to 7.6%, 2.7% and 1.7% by increasing the volume fraction to $\phi = 1\%, 5\%$ and 10%. At low ϕ, it has been previously shown that the interaction between particles and turbulence is important [13]. Particle wakes are quickly disrupted and the particles boundary layers are modified, resulting in the onset of unsteady effects that increase the overall drag. However, as ϕ increases, the hindering effect is also enhanced. This can be seen from figure 1(b) where the mean fluid speed in the gravity direction is shown. For both quiescent and turbulent cases, the mean fluid speeds $\langle V_{f,z} \rangle$ are normalized by the values obtained for $\phi = 0.5\%$ (the actual values of $\langle V_{f,z} \rangle / V_t$ are shown in the inset of the same figure). We see that in the densest case ($\phi = 10\%$), the mean fluid speed $\langle V_{f,z} \rangle$ is 15 times larger than that for $\phi = 0.5\%$. Due to the large hindrance, the effect of turbulence on the settling speed is reduced and therefore $\langle V_{p,z} \rangle$ is similar in both HIT and quiescent fluid.

We then report the probability density functions, $p.d.f.$s, of particle velocities in the directions parallel and perpendicular to gravity, $V_{p,z}$ and $V_{p,x}$ (since the settling occurs symmetricaly around the vertical direction, we report only one component of the particle lateral velocity). The former are shown in figures 2(a,b) for turbulent and quiescent cases. The first four central moments of these $p.d.f.$s are given in table 2. In HIT, we see that for $\phi \leq 1\%$, $p.d.f.$s are approximately symmetric around the mean values ($S_{V_{p,z}} \simeq 0$), see figure 2(a). For larger ϕ the variance $\sigma^2_{V_{p,z}}$ is basically unaltered, showing that the interaction with turbulence still governs the second order moment (i.e., the particle velocity fluctuations). On the contrary, the skewness $S_{V_{p,z}}$ attains finite positive values and increases with ϕ. This suggests that velocities substantially larger than the mean are seldomly reached, due to the stronger hindering effect. Interestingly, the $p.d.f.$s for both quiescent and turbulent cases at $\phi = 10\%$
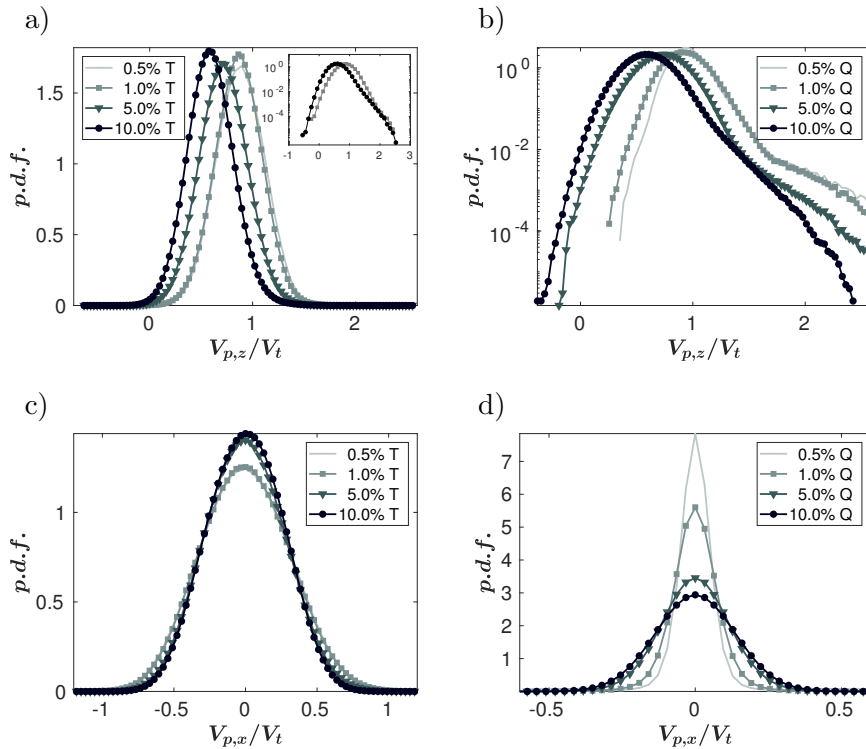
Fig. 2 The probability density function of the settling speed $V_{p,z}$ for all ϕ: (a) turbulent cases; (b) quiescent cases (in lin-log scale). The inset of panel (a) shows the $p.d.f.$s of the turbulent cases with $\phi = 1\%$ and 10% in lin-log scale. The probability density function of the particles speed in the direction perpendicular to gravity, $V_{p,x}$, for all ϕ: (c) turbulent cases; (d) quiescent cases.

are similar. From table 2 we can also appreciate the similarity between the central moments of the $p.d.f.$s, at both $\phi = 5\%$ and 10%. Clearly, due to the interaction with turbulence, the variance is enhanced while the skewness is reduced.

If we look at the results for the quiescent cases (figure 2b), we see that especially at low ϕ the $p.d.f.$s are highly skewed with strong positive tails. As discussed in Fornari et al. [13], these are related to frequent drafting-kissing-tumbling events. At large ϕ, however, particle wakes are more quickly disrupted by the increased presence of neighbor particles and these events become less frequent. In addition, due to the strong hindrance large velocities are not often reached. Hence, the tails of the $p.d.f.$s become progressively less intense by increasing ϕ (i.e., both $S_{V_{p,z}}$ and $K_{V_{p,z}}$ are smaller for $\phi = 5\%, 10\%$ than for $\phi = 0.5\%, 1\%$).

Concerning the $p.d.f.$s of lateral velocities, $V_{p,x}$, shown in figures 2(c,d), we see that they are centered around a zero mean (with a statistical error of, at

Quiescent	$\phi = 0.5\%$	$\phi = 1\%$	$\phi = 5\%$	$\phi = 10\%$
$\langle V_{p,z} \rangle$	$+0.96$	$+0.93$	$+0.74$	$+0.60$
$\sigma_{V_{p,z}}$	$+0.15$	$+0.17$	$+0.19$	$+0.20$
$S_{V_{p,z}}$	$+1.26$	$+0.70$	$+0.18$	$+0.33$
$K_{V_{p,z}}$	$+9.65$	$+6.01$	$+3.90$	$+4.01$
Turbulence	$\phi = 0.5\%$	$\phi = 1\%$	$\phi = 5\%$	$\phi = 10\%$
$\langle V_{p,z} \rangle$	$+0.88$	$+0.86$	$+0.72$	$+0.59$
$\sigma_{V_{p,z}}$	$+0.23$	$+0.23$	$+0.24$	$+0.23$
$S_{V_{p,z}}$	$+0.01$	$+0.01$	$+0.11$	$+0.23$
$K_{V_{p,z}}$	$+2.92$	$+3.15$	$+3.31$	$+3.47$

Table 2 First four central moments of the probability density functions of $V_{p,z}$ normalized by V_t. $S_{V_{p,z}}$ and $K_{V_{p,z}}$ are respectively the skewness and the flatness of the $p.d.f.$s. The moments of the $p.d.f.$s pertaining to the quiescent cases are reported first. Results for turbulent cases follow.
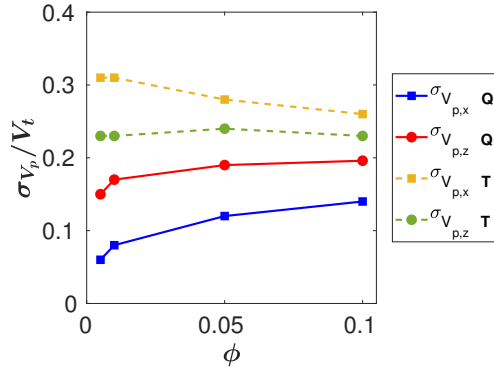
Fig. 3 Comparison of the root-mean-square particle velocities, σ_{V_p}, for all ϕ. Turbulent and quiescent cases are labeled with **T** and **Q**, respectively.

most, $O(10^{-3})$). The main effect of the turbulence is here to highly enhance the standard deviation of the $p.d.f.$s, especially at low ϕ. The standard deviation $\sigma_{V_{p,x}}$ is $0.31, 0.31, 0.28$ and 0.26 for the turbulent cases with $\phi = 0.5\%, 1\%, 5\%$ and 10%. For the quiescent cases we find instead $\sigma_{V_{p,x}} = 0.06, 0.08, 0.12$ and 0.14, respectively. We see that for $\phi = 0.5\%$, $\sigma_{V_{p,x}}$ is approximately 5 times larger in turbulence than in quiescent fluid. However, the difference in $\sigma_{V_{p,x}}$ decreases with ϕ and, for $\phi = 10\%$, $\sigma_{V_{p,x}}$ is only ~ 2 times larger in HIT. This may be due to the fact that at large ϕ, particles are surrounded by many neighbors and their lateral motion is hence hindered (due to lubrication and collisions). In figure 3 we report the variation with ϕ of the standard deviations of the velocities in the directions parallel and perpendicular to gravity for all cases studied. We see that in quiescent fluid, $\sigma_{V_{p,x}}$ and $\sigma_{V_{p,z}}$ increase with ϕ. On the other hand, in HIT $\sigma_{V_{p,z}}$ is approximately constant, while $\sigma_{V_{p,x}}$ decreases for $\phi > 1\%$. The anisotropy of velocity fluctuations, $\sigma_{V_{p,x}}/\sigma_{V_{p,z}}$, hence decreases for turbulent cases (from 1.35 to 1.13), while it increases in quiescent fluid (from 0.4 to 0.7). It can be expected that by further increasing ϕ, the
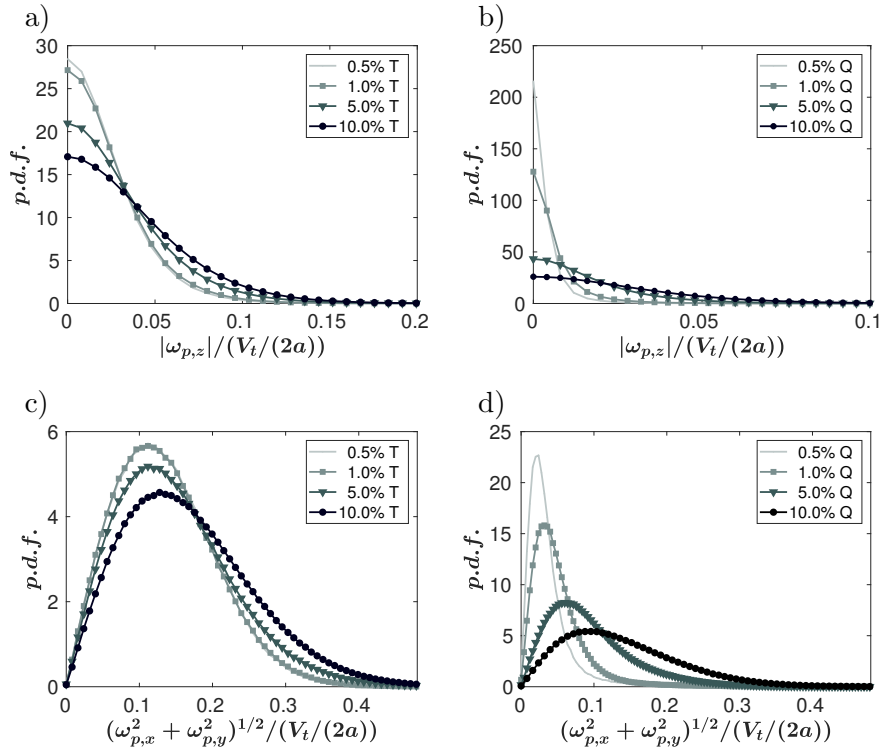
Fig. 4 The probability density functions, *p.d.f.*s, of the absolute value of the particle angular velocities in the direction of gravity, $|\omega_{p,z}|$, for turbulent (a) and quiescent cases (b). The *p.d.f.*s of $\sqrt{\omega_{p,x}^2 + \omega_{p,y}^2}$ (the magnitude of the angular velocity in the directions perpendicular to gravity) for turbulent (c) and quiescent cases (d).

anisotropy $\sigma_{V_{p,x}}/\sigma_{V_{p,z}}$ will eventually converge to 1 in both HIT and quiescent fluid. This behavior is reasonable because at higher ϕ due to relatively smaller void regions, there will be higher particle-particle interactions that promote similar velocity fluctuations in all directions leading to a smaller anisotropy.

We now turn to the discussion of the probability density functions of the particle angular velocities normalized by $V_t/(2a)$. Figure 4(a) shows the *p.d.f.*s of the absolute value of the particle angular velocities in the direction of gravity, $|\omega_{p,z}|$, in HIT. We see that both the mean value and the variance of $|\omega_{p,z}|$ increase with ϕ. It should be noted, however, that the mean angular velocity in the direction of gravity $\omega_{p,z}$ is null (as in the other directions) and for this reason we are considering the absolute value. At larger ϕ, particle-particle interactions increase leading to larger $|\omega_{p,z}|$. The same is observed in quiescent fluid (figure 4b), although the mean value and variance of $|\omega_{p,z}|$ increase more drastically. The particle mean rotation around z is indeed negligible for $\phi = 0.5\%$ ($\langle|\omega_{p,z}|\rangle = 0.004$), while it is ~ 7 times larger for $\phi = 10\%$ ($\langle|\omega_{p,z}|\rangle = 0.027$).
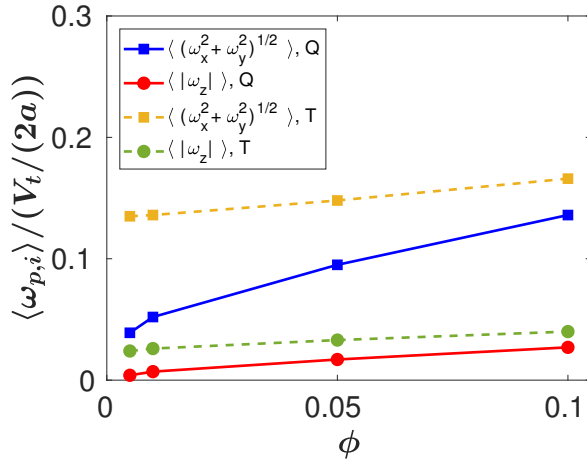
Fig. 5 Particle angular velocity: variation with ϕ of the mean values of $|\omega_{p,z}|$ and $\sqrt{\omega_{p,x}^2 + \omega_{p,y}^2}$ for both turbulent ($\boldsymbol{T}$) and quiescent ($\boldsymbol{Q}$) cases.

In figures 4(c,d) we show instead the $p.d.f.$s of the magnitude of the angular velocities in the direction perpendicular to gravity, $\sqrt{\omega_{p,x}^2 + \omega_{p,y}^2}$, for turbulent and quiescent cases. These are also normalized by $V_t/(2a)$. Again, the mean and the variance increase with ϕ, especially in quiescent fluid. Indeed, for $\phi = 0.5\%$, $\langle \sqrt{\omega_{p,x}^2 + \omega_{p,y}^2} \rangle = 0.039$ while for $\phi = 10\%$, $\langle \sqrt{\omega_{p,x}^2 + \omega_{p,y}^2} \rangle = 0.136$ (in quiescent fluid). The mean values and standard deviations of $|\omega_{p,z}|$ and $\sqrt{\omega_{p,x}^2 + \omega_{p,y}^2}$ are reported in table 3. It is also interesting to note that in HIT, the $p.d.f.$s of $|\omega_{p,z}|$ and $\sqrt{\omega_{p,x}^2 + \omega_{p,y}^2}$ are almost prefectly overlapped (see figure 4c), suggesting again that at small ϕ turbulent fluctuations dominate the dynamics.

The mean values of $|\omega_{p,z}|$ and $\sqrt{\omega_{p,x}^2 + \omega_{p,y}^2}$ are also shown in figure 5 as function of ϕ, for both quiescent and turbulent cases. As for the particle linear velocities, we clearly see that by increasing ϕ the mean values for quiescent and turbulent cases become similar. Hence, also the particle angular velocity dynamics deeply depends on excluded volume effects, especially at large ϕ. At low ϕ, particle rotation is substantially larger in HIT than in quiescent fluid. Indeed, in the latter case, moving particles are the only cause of fluid rotation, i.e. vorticity. Therefore, at low concentration $\phi = 0.5 - 1\%$ under quiescent conditions, the distribution of particle rotation is very narrow as it is weakly affected by the small fluctuations of the fluid velocity and by rare particle-particle interactions. On the other hand, under turbulent conditions, even at low concentration the distribution of particle rotation has a larger

Quiescent	$\phi = 0.5\%$	$\phi = 1\%$	$\phi = 5\%$	$\phi = 10\%$
$\langle|\omega_{p,z}|\rangle$	+0.004	+0.007	+0.017	+0.027
$\sigma_{|\omega_{p,z}|}$	+0.006	+0.008	+0.016	+0.022
Turbulence	$\phi = 0.5\%$	$\phi = 1\%$	$\phi = 5\%$	$\phi = 10\%$
$\langle|\omega_{p,z}|\rangle$	+0.024	+0.026	+0.033	+0.040
$\sigma_{|\omega_{p,z}|}$	+0.021	+0.022	+0.028	+0.032
Quiescent	$\phi = 0.5\%$	$\phi = 1\%$	$\phi = 5\%$	$\phi = 10\%$
$\langle\sqrt{\omega_{p,x}^2 + \omega_{p,y}^2}\rangle$	+0.039	+0.052	+0.095	+0.136
$\sigma_{\sqrt{\omega_{p,x}^2+\omega_{p,y}^2}}$	+0.038	+0.041	+0.061	+0.078
Turbulence	$\phi = 0.5\%$	$\phi = 1\%$	$\phi = 5\%$	$\phi = 10\%$
$\langle\sqrt{\omega_{p,x}^2 + \omega_{p,y}^2}\rangle$	+0.135	+0.136	+0.148	+0.166
$\sigma_{\sqrt{\omega_{p,x}^2+\omega_{p,y}^2}}$	+0.068	+0.070	+0.079	+0.088

Table 3 Mean and standard deviation of $|\omega_{p,z}|$ and $\sqrt{\omega_{p,x}^2 + \omega_{p,y}^2}$ (normalized by $V_t/(2a)$) for all ϕ. First, the results for $|\omega_{p,z}|$ in quiescent fluid and turbulence are shown. These are followed by the results for $\sqrt{\omega_{p,x}^2 + \omega_{p,y}^2}$ for both quiescent and turbulent cases.

variance induced by the strong fluid velocity turbulent fluctuations. If we consider the unladen reference case in HIT, we find that the standard deviation of the vorticity is $\sigma_{\Omega_f}(2a)/V_t = 0.44$ or, in terms of the fluid angular velocity, $\sigma_{\omega_f} = 0.5\sigma_{\Omega_f} = 0.22$. Hence, in these conditions the environmental fluid itself has large rotational velocity fluctuations that force particle rotation. As a consequence, the intrinsic rotationality of the flow (in turbulence) leads to a larger particle rotation than in quiescent fluid.

4 Particle velocity correlations and mean square displacements

In the last section we have reported single-point statistics related to the particle linear and angular velocities. Now instead, we turn to the discussion of the temporal correlations of the particle velocity fluctuations:

$$R_{v_x v_x}(\Delta t) = \frac{\langle V'_{p,x}(p,t)V'_{p,x}(p,t+\Delta t)\rangle}{\sigma^2_{V_{p,x}}} \tag{6}$$

$$R_{v_z v_z}(\Delta t) = \frac{\langle V'_{p,z}(p,t)V'_{p,z}(p,t+\Delta t)\rangle}{\sigma^2_{V_{p,z}}} \tag{7}$$

The correlations in the direction perpendicular to gravity are shown in figures 6(a,b) for turbulent and quiescent cases. We generally find that $R_{v_x v_x} = 0$ is reached more quickly in HIT than in quiescent fluid. However, while in the quiescent cases $R_{v_x v_x} \simeq 0$ for all Δt, once decorrelation has occured, in HIT the velocity correlation oscillates around zero before finally converging to $R_{v_x v_x} = 0$ (for $\Delta t \geq 50\,(2a)/V_t$). For $\phi = 0.5\%, 1\%$ the initial period of oscillation of $R_{v_x v_x}$ is similar and of about $16\,(2a)/V_t$. Following the concept of crossing trajectories [8], the period of oscillation of the fluctuations can

a)

b)

c)

d)
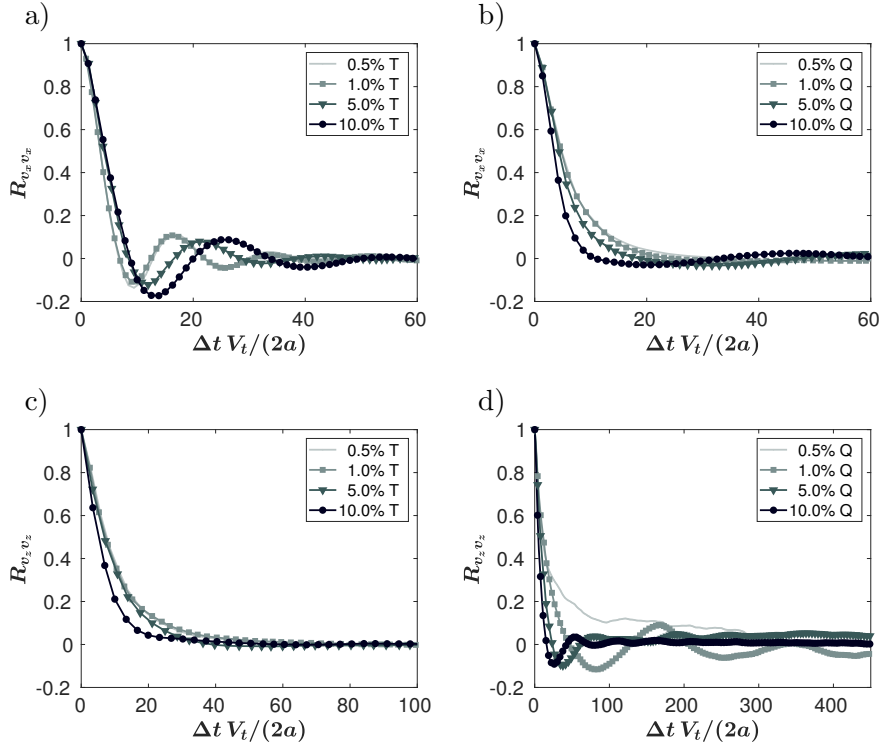
Fig. 6 Time correlations of the particle velocity fluctuations. Panels (a) and (b) show the correlations of $V'_{p,x}$ for all ϕ, in HIT and in quiescent fluid. Instead, panels (c) and (d) show the correlations of $V'_{p,z}$ for all ϕ, in HIT and in quiescent fluid.

be defined as the ratio between the typical eddy diameter in the direction of gravity (i.e., the integral lengthscale L_0) and the characteristic particle (terminal) velocity V_t. From this we obtain $t_{osc} \simeq 16$ which matches our result. By increasing ϕ we see that the zero crossing is retarded, and the oscillation period is increased up to $\approx 26 \,(2a)/V_t$ for $\phi = 10\%$. This suggests that at large ϕ particles respond less to turbulence-induced disturbances. In quiescent fluid, we find instead that $R_{v_x v_x}$ decreases more rapidly at larger ϕ. Indeed, at large ϕ each particle is surrounded by many neighbours. Therefore, if it moves laterally it probably collides with another particle and is quickly slowed down, resulting in an earlier decorrelation of the velocity fluctuations.

The correlations in the direction parallel to gravity, $R_{v_z v_z}$, are instead shown in figures 6(c,d) for turbulent and quiescent cases. It is clear that for $\phi = 0.5\%$, velocity fluctuations $V'_{p,z}$ decorrelate faster in HIT than in quiescent fluid. This is because at low ϕ particles either fall undisturbed along gravity, or interact with other particles being quickly accelerated in their wakes (drafting-kissing-tumbling). Hence, vertical velocity fluctuations are correlated for very long times. In constrast, in HIT the turbulence strongly alters the fluid velocity

field seen by the particles, and rapidly disrupts their wakes. Particles may even resuspend when they encounter very intense vortices. Consequently, the vertical velocity fluctuations decorrelate substantially faster than in quiescent fluid ($\Delta \sim 50/60\,(2a)/V_t$).

In HIT, the vertical velocity correlations $R_{v_z v_z}$ are similar for all ϕ, although it appears that decorrelation is reached slightly earlier at larger ϕ ($\Delta \sim 40/50\,(2a)/V_t$). An interesting change in $R_{v_z v_z}$ is instead observed for quiescent cases. As said, for $\phi = 0.5\%$, very long times are needed for decorrelation to occur. For $\phi = 1\%$, we see instead that $R_{v_z v_z}$ crosses the null value more rapidly ($\Delta t \simeq 48\,(2a)/V_t$), and it then oscillates around it with decreasing amplitude. By further increasing ϕ, we see that the zero-crossing is anticipated and that the extent of the oscillations is substantially reduced. Therefore, the case at $\phi = 1\%$ appears as a transition between a regime where particle-particle interactions are rare and intermittent (i.e., the drafting-kissing-tumbling at low ϕ), and the dynamics is almost only governed by buoyancy, and a regime where particle-particle interactions (lubrication and collisions) and hindrance are intense and control the dynamics. Notice also that for $\phi \leq 5\%$, the correlation $R_{v_z v_z}$ crosses the null value more quickly in quiescent fluid than in HIT.

To further understand the dynamics of the solid phase, we calculate the mean square displacement of the particles,

$$\langle \mathbf{x}^2 \rangle(\Delta t) = \langle [\mathbf{x}_p(t + \Delta t) - \mathbf{x}_p(t)]^2 \rangle. \tag{8}$$

Notice that in the falling direction we have subtracted the mean displacement, $\langle V_{p,z} \rangle t$, from the instantaneous displacement, $\Delta z_p(t)$, to highlight the fluctuations with respect to the mean motion.

The mean square displacement in the direction perpendicular to gravity, $\langle \Delta x^2 \rangle$, is shown in figures 7(a,b) for turbulent and quiescent cases. For both cases we initially find a quadratic (ballistic) scaling in time ($\langle \Delta x^2 \rangle \sim t^2$) typical of correlated motions, and a linear diffusive scaling at long times ($\langle \Delta x^2 \rangle \sim 2 D_e t$, with D_e the diffusion coefficient). The crossover time between the two regimes is approximtely $10/20\,(2a)/V_t$ for the turbulent cases, while it decreases with ϕ from $\sim 50\,(2a)/V_t$ to $\sim 20\,(2a)/V_t$ for the quiescent cases. In HIT, the mean square displacement $\langle \Delta x^2 \rangle$ is similar for $\phi \leq 5\%$. For $\phi = 10\%$ it is slightly smaller in both the ballistic and diffusive regimes. This can also be noted from the diffusion coefficients, D_e, reported in table 4. We see that D_e reaches a maximum for $\phi = 1\%$ ($D_e \simeq 0.32$). On the other hand, the value for $\phi = 10\%$ ($D_e \simeq 0.22$) is even smaller than that at $\phi = 0.5\%$. The dispersion is hence less effective at large ϕ. For the quiescent cases we observe instead that the lateral dispersion increases with ϕ. The diffusion coefficient, D_e, increases from about 0.03 for $\phi = 0.5\%, 1\%$, to 0.05 for $\phi = 5\%, 10\%$ (clearly the dispersion rate is smaller than in HIT). At low ϕ, particles mostly fall vertically and rarely interact with each other. On the contrary, at large ϕ they interact substantially with surrounding particles (both hydrodynamically and via collisions), and this results in a more efficient lateral dispersion.

Finally, the vertical mean square displacement, $\langle \Delta z^2 \rangle$, is shown in figures 7(c,d) for turbulent and quiescent cases. As discussed above, the mean

a)

b)

c)

d)
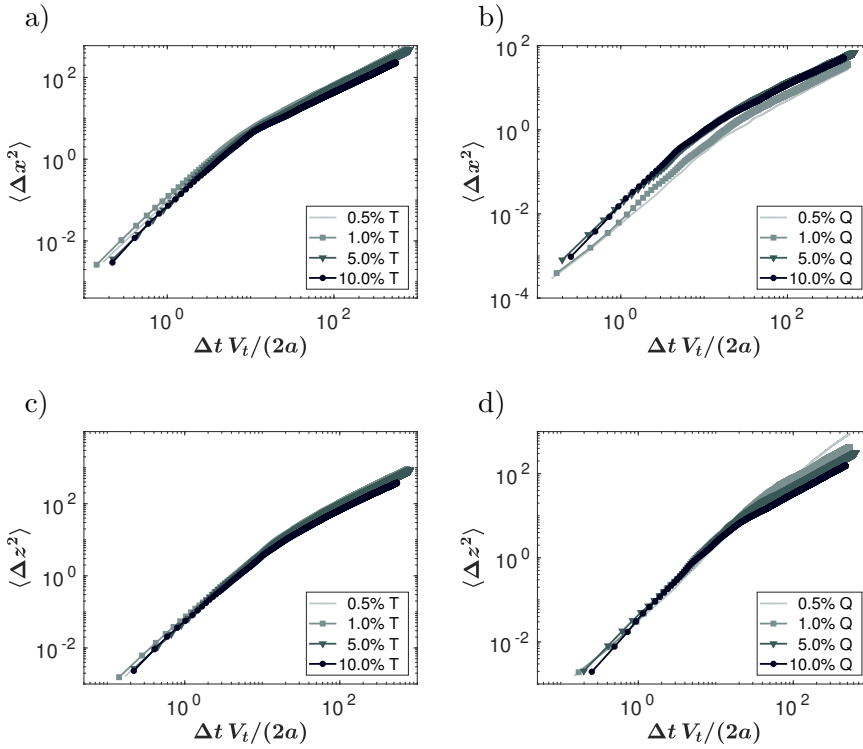
Fig. 7 Panels (a) and (b) show the mean square particle displacement in the direction perpendicular to gravity, $\langle \Delta x^2 \rangle$, for all ϕ, in HIT and in quiescent fluid. Instead, panels (c) and (d) show the mean square particle displacement in the direction parallel to gravity, $\langle \Delta z^2 \rangle$, for all ϕ, in HIT and in quiescent fluid.

Quiescent	$\phi = 0.5\%$	$\phi = 1\%$	$\phi = 5\%$	$\phi = 10\%$
$D_e(\langle \Delta x^2 \rangle)$	0.03	0.03	0.05	0.05
$D_e(\langle \Delta z^2 \rangle)$	$--$	0.40	0.24	0.17
Turbulence	$\phi = 0.5\%$	$\phi = 1\%$	$\phi = 5\%$	$\phi = 10\%$
$D_e(\langle \Delta x^2 \rangle)$	0.28	0.32	0.29	0.22
$D_e(\langle \Delta z^2 \rangle)$	0.52	0.57	0.52	0.35

Table 4 The diffusion coefficients, $D_e = \langle \Delta \mathbf{x}^2 \rangle/(2\Delta t)$, in the directions perpendicular and parallel to gravity, for all quiescent and turbulent cases.

square displacement is increased by the interaction with the turbulence. However, we see that in the direction of gravity dispersion is mostly governed by buoyancy and hindrance and, consequently, the increase in $\langle \Delta z^2 \rangle$ with respect to quiescent cases is smaller than for $\langle \Delta x^2 \rangle$. This can also be seen from the diffusion coefficients, D_e, reported in table 4. Notice that the full diffusive behavior has not yet been reached for the most diluted quiescent case and, therefore, no diffusion coefficient is reported. As found for $\langle \Delta x^2 \rangle$, in HIT the

diffusion coefficient reaches a maximum for $\phi = 1\%$ ($D_e = 0.57$). The value for $\phi = 10\%$ ($D_e = 0.35$) is instead substantially smaller than that for $\phi = 0.5\%$. The diffusion coefficient decreases with ϕ also for the quiescent cases ($\phi \geq 1\%$), differently from what observed for the lateral dispersion. Hence, in both HIT and quiescent fluid, particle-particle interactions and hindrance reduce particle dispersion in the gravity direction, especially at large ϕ.

5 Particle-pair statistics

In this last section we examine particle-pair statistics as function of the radial distance between particle centers, $r/(2a)$. We have previously mentioned the importance of particle-particle interactions (lubrications and collisions), and it is therefore interesting to investigate how the particle-pair dynamics changes with ϕ, in HIT and quiescent fluid.

An indicator of the radial separation among pair of particles is the radial distribution function $g(r)$. In a reference frame with origin at the centre of a particle, the $g(r)$ is the average number of particle centers located in the shell of radius r and thickness Δr, normalized with the number of particles of a random distribution. Formally, the radial distribution function is defined as

$$g(r) = \frac{1}{4\pi} \frac{dN_r}{dr} \frac{1}{r^2 n_0}, \tag{9}$$

where N_r is the number of particle pairs on a sphere of radius r, and $n_0 = N_p(N_p - 1)/(2V)$ is the density of particle pairs in the volume V (N_p the total number of particles). The value of $g(r)$ at distances of the order of the particle diameter reveals the intensity of clustering. Instead, for $r \to \infty$ the radial distribution function, $g(r)$, tends to 1, corresponding to a random (Poissonian) distribution.

The radial distribution function, $g(r)$, is shown in figure 8(a) for all turbulent cases. At low $\phi \leq 1\%$, the value at contact is small ($g(r = 2a) \simeq 1.7$) indicating that there is a low extent of clustering. The radial distribution function then rapidly drops to values smaller than 1. Hence, for radial distances ($r/(2a)$) between 1.01 and 1.7, it is very unlikely to find particle-pairs. For larger $r/(2a)$, $g(r) = 1$ (i.e., there is an uniform distribution of particles). Increasing ϕ, we see that the region where $g(r) < 1$ progressively disappears, and that the maximum value at contact increases ($g(r = 2a) \simeq 4$ for $\phi = 10\%$). Hence, at large ϕ there is a (slightly) higher probability of finding particle-pairs for $r/(2a) = 1$, while particle distribution becomes more quickly uniform.

The results for the quiescent cases are instead shown in figure 8(b). The maximum of $g(r)$ now exhibits a non-monotonic behavior with ϕ. For $\phi = 0.5\%$, $g(r = 2a)$ is largest ($\simeq 5.3$). The larger extent of clustering is due to frequent drafting-kissing-tumbling events, see also [13]. By increasing $r/(2a)$, the radial distribution function quickly drops to values smaller than 1. The uniform distribution ($g(r) = 1$) is found at large distances, $r/(2a) > 3.3$. This is larger than in HIT, since particles are not mixed by turbulence and only interact

through their wakes. By increasing ϕ, the maximum of $g(r)$ first decreases to $\simeq 2$ for $\phi = 5\%$, and it then increases again to $\simeq 3.9$ for $\phi = 10\%$. At $\phi = 10\%$, the $g(r)$ is very similar to that of the turbulent case. Hence, at large ϕ turbulence mixing is less efficient and the particle distribution is strictly related to hydrodynamic interactions and collisions (i.e., to particle-particle interactions).

We then show in figures 8(c) and (d), the averaged normal relative velocity between two approaching particles. This is obtained as the projection of the relative velocity in the direction of the distance between the two interacting particles

$$dV_n(r_{ij}) = (\mathbf{V}_i - \mathbf{V}_j) \cdot \frac{(\mathbf{r}_i - \mathbf{r}_j)}{|(\mathbf{r}_i - \mathbf{r}_j)|} = (\mathbf{V}_i - \mathbf{V}_j) \cdot \frac{\mathbf{r}_{ij}}{|\mathbf{r}_{ij}|} \qquad (10)$$

(where i and j denote the two particles). This scalar quantity can be either positive (when two particles depart form each other) or negative (when they approach). Hence, the averaged normal relative velocity can be decomposed into $\langle dV_n(r) \rangle = \langle dV_n^+(r) \rangle + \langle dV_n^-(r) \rangle$. To estimate the probability of a collision, the mean negative normal relative velocity is therefore needed. For sake of simplicity we denote the latter as $w(r)/V_t$ and we show the absolute value.

From figure 8(c) we see that $w(r)/V_t$ is similar at contact ($r/(2a) = 1$) and for $r/(2a) > 3.5$, for all turbulent cases. At contact, $w(r = 2a)/V_t$ increases from 0.014 (for $\phi = 0.5\%$) to 0.017 (for $\phi = 10\%$). Generally, $w(r)/V_t$ increases with ϕ, especially between $r/(2a) = 1.2$ and 3.5. This may be related to the fact that at low ϕ particles are typically far away from each other and rarely interact.

The mean negative normal relative velocity of the quiescent cases is instead shown in figure 8(d). There is a clear change in the profiles of $w(r)/V_t$ as ϕ increases from 1% to 5%. For $\phi = 0.5\%$ and 1% we see that $w(r)/V_t$ is particularly high between $r/(2a) = 1.06$ and 1.7. This may be related to the large acceleration that a particle experiences when it is drafted in the wake of another particle (i.e., during drafting-kissing-tumbling events). On the contrary, in denser cases ($\phi > 1\%$) particles wakes are quickly disrupted due to excluded volume effects, and the profiles of $w(r)/V_t$ increase (almost) monotonically. Exactly at contact, $w(r = 2a)/V_t$ increases from 0.011 (for $\phi = 0.5\%$) to 0.014 (for $\phi = 10\%$). The lower value of $w(r = 2a)/V_t$ for $\phi = 0.5\%$ suggests that although particles are highly accelerated as they are drafted in a wake, lubrication forces close to contact are strong and damp the motion of the upper particle, softening the collision. Finally, we observe that for $r/(2a) > 2.5$, $w(r)/V_t$ clearly increases with ϕ. Indeed, for $\phi \leq 1\%$ particles separated by 2.5 diameters (especially in the plane perpendicular to gravity) rarely interact.

To conclude this section, we report in figure 8(e) the collision frequency N_c for all cases examined. The general collision kernel is proportional to the product of the radial distribution function, $g(r)$, and the mean relative velocity,
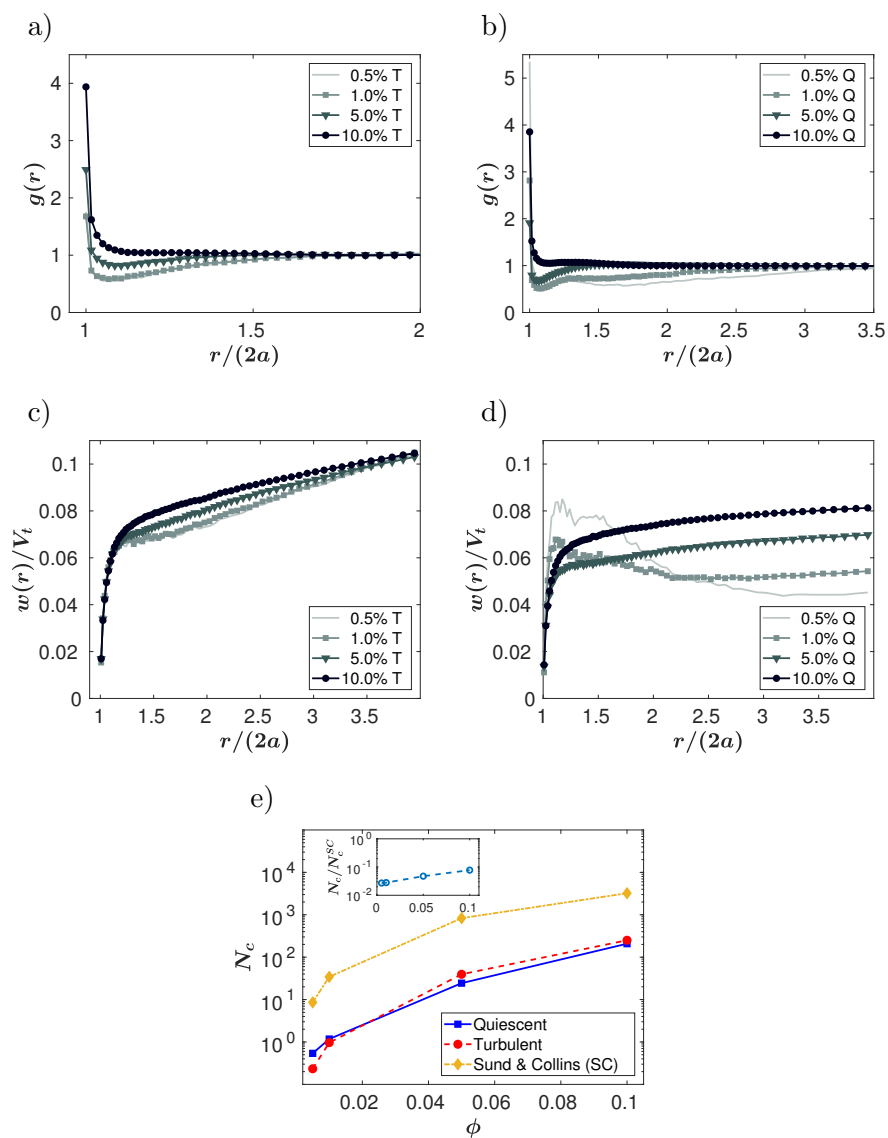
Fig. 8 The radial distribution function, $g(r)$, for all ϕ: in turbulence (a) and in quiescent fluid (b). The average (negative) relative velocity, $|w(r)/V_t|$ for all ϕ: in turbulence (c) and in quiescent fluid (d). The collision frequency at contact is shown in panel (e) for all cases. In the inset, we show the ratio between N_c and the estimate by Sundaram and Collins N_c^{SC} [31].

$w(r)/V_t$ [31]:

$$\kappa(r) \cong \frac{1}{2}\pi(2a)^2 \left(\frac{N_p}{V}\right)^2 g(r) \cdot |w(r)|. \qquad (11)$$

At contact (i.e., when $r = 2a$), equation 11 gives us the collision frequency, N_c. For inertial particles, smaller than the Kolmogorov length scale, uniformly distributed in space, Sundaram and Collins [31] derived the following estimate for the collision frequency:

$$N_c^{SC} = \frac{1}{2}(2a)^2 \left(\frac{N_p}{V}\right)^2 \left(\frac{16\pi\sigma_{V_p}^2}{3}\right)^{1/2}. \qquad (12)$$

To compare with our results, we have also estimated N_c^{SC} by replacing σ_{V_p} in equation 12, with the average of $\sigma_{V_{p,x}}$, $\sigma_{V_{p,y}}$ and $\sigma_{V_{p,z}}$.

From figure 8(e) we see that the collision frequency increases substantially with ϕ, both in HIT and in quiescent fluid. Interestingly, at low $\phi \le 1\%$ the collision frequency N_c is larger in the quiescent cases, rather than in HIT. Indeed, although $w(r = 2a)/V_t$ is slightly larger in HIT, we have previously seen that the extent of small-scale clustering is clearly larger in quiescent fluid (see figure 8a and b). Indeed, particle distribution is homogenized due to turbulence mixing, and the frequency of drafting-kissing-tumbling events is drastically reduced. This results in the reduction of N_c in HIT (at low ϕ). For comparison, we have also reported the estimate N_c^{SC}. This value alone overestimates the collision frequency in HIT. However, N_c appears to be almost proportional to N_c^{SC}. The important reduction of the apparent collision frequency with respect to the estimate of equation (12) can be interpreted as an effect of particle pair small scale interaction. The main assumption needed to determine eq. (12), that is far to be verified in the present cases, concerns the uncorrelated relative particle motion at all scales. In particular, as shown in panels (c) and (d) of figure 8 the relative approaching velocity suddenly drops near the particle pair contact. This mechanism is induced by the strong lubrication forces that develop at small separations slowing down the particle approaching velocity which becomes much lower than the particle velocity variance. The effect of the lubrication forces is expected to reduce its importance when the particle density becomes higher, but cannot be neglected for almost neutrally buoyant particles, as shown in the present study.

For $\phi \ge 5\%$, N_c becomes larger in HIT than in quiescent fluid. Indeed, the normal relative velocity $w(r = 2a)/V_t$ is higher in HIT than in quiescent fluid, while the extent of clustering is similar, especially for $\phi = 10\%$. As for the cases at low ϕ, the collision frequency N_c is lower than the estimate N_c^{SC}. However, the ratio N_c/N_c^{SC} increases with ϕ, as can be seen from the inset of figure 8(e). Indeed, while the increase with ϕ of the average relative velocity is small, at large volume fractions there is a substantially larger probability of finding particle-pairs. The larger $g(r)$ at contact is responsible for the larger N_c^{SC}.

6 Fluid phase statistics in the turbulent regimes

To better understand the effect of the volume fraction on the interaction between particles and fluid, we report some relevant statistics characterizing the fluid phase in the turbulent regime.

In particular, the Reynolds number based on the Taylor microscale, Re_λ, the mean energy dissipation ϵ, and the fluid velocity fluctuation intensities in the directions parallel and perpendicular to gravity, u'_x and u'_y, are reported in figure 9(a,b,c). Concerning the Taylor Reynolds number we note that it decreases monotonically with ϕ, and at $\phi = 10\%$ Re_λ becomes one third of the value of the unladen case; see figure 9(a). This is mostly due to a strong enhancement of the energy dissipation with ϕ, that in turn leads to a reduction of the Taylor microscale λ.

The variation of the mean energy dissipation, ϵ, as function of the volume fraction is shown in figure 9(b). We observe that ϵ increases almost linearly with ϕ. Indeed, at $\phi = 10\%$ the mean energy dissipation is approximately 10 times that of the unladen case. The increase of the amount of energy to be dissipated is promptly explained considering that settling particles are forced by gravity which is a source of energy. This additional energy injection is transferred by particles to the fluid at the particle scale through their wakes. Associated with this energy input there is also a new dissipative mechanism. This is related to the large shear generated at the particles surfaces due to the no-slip boundary conditions [37, 13]. The results show that the additional energy input/dissipation due to the settling particles strongly increases with ϕ, and quickly becomes the dominant contribution to the overall energy dissipation.

Finally, in figure 9(c) we show the mean fluid velocity fluctuation intensities (rms) in the directions parallel (u'_z) and perpendicular to gravity (u'_x). Concerning u'_x, we find that it decreases from 0.3 to about 0.26 as ϕ is increased from 0 to $0.5 - 1\%$. Hence, due to the presence of the solid particles, the transversal turbulent eddies are quickly attenuated leading to a 13% reduction in u'_x. Further increasing the volume fraction ϕ, u'_x slightly decreases to ~ 0.25. We then notice that in the direction parallel to gravity, the velocity fluctuations are larger than the corresponding u'_x, and substantially increase with ϕ. Generally, $u'_z > u'_x$ due to the fact that energy is injected from the wakes of the settling particles. At $\phi = 0.5\%$, u'_z is approximately 8.5% smaller than the nominal velocity fluctuation of the single phase simulation, u'. Further increasing ϕ, u'_z rapidly grows becoming larger than the nominal u' (of the unladen case) for $\phi \geq 2\%$. As previously mentioned, at large ϕ hindrance becomes the dominant effect, leading to the reduction of the mean settling speed, and to the strong enhancement of the vertical mean and fluctuating velocity.

a)

b)

c)
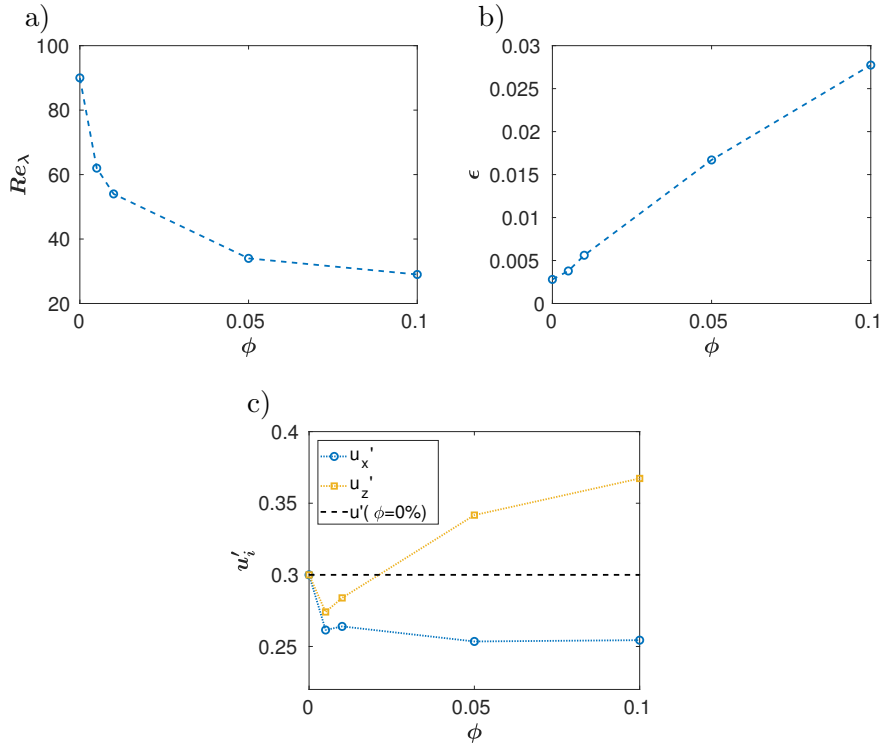
Fig. 9 (a) The evolution of the Reynolds number based on the Taylor microscale as function of the volume fraction ϕ. (b) The evolution of the mean energy dissipation ϵ as function of the volume fraction ϕ. (c) The fluid velocity fluctuations (rms) in the directions parallel (u'_z) and perpendicular (u'_x) to gravity as function of ϕ. The black dashed line represents the turbulent velocity fluctuations of the unladen case.

7 Final remarks

We have studied the sedimentation of finite-size particles in homogeneous isotropic turbulence and in quiescent fluid via Direct Numerical Simulations. In particular, we have considered rigid spherical particles slightly heavier than the fluid ($R = 1.02$), with Galileo number $Ga = 145$, and with solid volume fractions $\phi = 0.5\%, 1\%, 5\%$ and 10%. We have found that the mean settling speed, $\langle V_{p,z} \rangle$ is always smaller in HIT than in quiescent fluid. However, the reduction in $\langle V_{p,z} \rangle$ (with respect to quiescent fluid), decreases by increasing particle concentration. Indeed, for $\phi = 0.5\%$, $\langle V_{p,z} \rangle$ is 8.3% smaller than in quiescent fluid, but for $\phi = 10\%$ the difference is only about 1.7%. At low ϕ, particles interact strongly with turbulence; their boundary layer is modified and their wakes are quickly disrupted. Hence, the clear change in dynamics with respect to what is observed in quiescent fluid. However, by increasing ϕ the hindering effect substantially increases. Notice that for $\phi = 10\%$, this is 15

times stronger than in the most dilute case ($\phi = 0.5\%$). Therefore, the effect of turbulence on the mean settling speed is reduced and $\langle V_{p,z} \rangle$ is similar in both HIT and quiescent fluid. While the mean settling speed becomes progressively dominated by hindrance, the particle velocity fluctuations in the gravity direction are always governed by turbulence. Consequently, $\sigma_{V_{p,z}}$ is similar for all ϕ.

We have then looked at the probability density functions, $p.d.f$.s, of the settling speeds. At low concentrations, $p.d.f$.s of $V_{p,z}$ are clearly different in HIT and quiescent fluid. In the former case, due to turbulence mixing, these are almost symmetric around the mean value, with a large standard deviation, $\sigma_{V_{p,z}}$. Instead, in quiescent fluid these are highly skewed towards larger velocities than the mean (due to frequent drafting-kissing-tumbling interactions), and their standard deviations, $\sigma_{V_{p,z}}$, are smaller than in HIT. On the other hand, for $\phi = 10\%$ the $p.d.f$.s are similar in both cases, since the strong hindering effect avoids particles from reaching very large velocities.

Concerning the $p.d.f$.s of the velocity perpendicular to gravity, $V_{p,x}$, we have seen that the variance is substantially larger in HIT than in quiescent fluid. As said, however, the effect of the turbulence decreases while increasing the concentration and, consequently, the variance ($\sigma^2_{V_{p,x}}$) progressively reduces. In quiescent fluid instead, at low ϕ particles interact mostly vertically and intermittently, and hence the variance $\sigma^2_{V_{p,x}}$ is small. At large ϕ, each particle is surrounded by many neighbors. Therefore, particle-particle interactions occur frequently and $\sigma^2_{V_{p,x}}$ increases.

From the $p.d.f$.s of the angular velocities, we have found that the mean values and the variance increase with ϕ, for both quiescent and turbulent cases. The relative increase in rotation rate is substantially larger in quiescent fluid than in HIT. It is indeed observed that the components of the angular velocity perpendicular to gravity approach those found in HIT.

We have then looked at the correlations of particle velocity fluctuations, $R_{v_x v_x}$ and $R_{v_z v_z}$. In the direction parallel to gravity, velocity fluctuations are found to decorrelate more quickly as ϕ increases. The decorrelation is faster in HIT at low ϕ. Indeed, due to particle interactions through wakes (i.e., drafting-kissing-tumbling events) it takes a long time for vertical velocity fluctuations to decorrelate in quiescent fluid. In the latter cases, we have also noticed that there is change in regime as ϕ increases above 1%. Indeed, for $\phi = 1\%$, $R_{v_z v_z}$ oscillates around zero (with decreasing amplitude). For larger ϕ the decorrelation is faster (even respect to turbulent cases), and $R_{v_z v_z}$ quickly converges to zero (after few oscillations). In HIT, the velocity correlations in the direction parallel to gravity initially oscillate around zero. The period of oscillation appears to be proportional to L_0/V_t, where L_0 and V_t are the integral lengthscale of the turbulence and the particle terminal velocity (see [8]). The period of oscillation increases with ϕ.

Concerning the particle mean square displacement, we have seen that $\langle \Delta x^2 \rangle$ is substantially larger in HIT, due to the mixing nature of the turbulence. The diffusion coefficient for $\langle \Delta x^2 \rangle$ is found to increase with ϕ in quiescent fluid. However, in HIT it reaches a maximum for $\phi = 1\%$, while the value

for $\phi = 10\%$ is smaller than that at $\phi = 0.5\%$. When the concentration is large, although particles are swept by turbulent eddies, they are hindered by surrounding particles. In the direction parallel to gravity, buoyancy and hindrance dominate the dynamics, and the difference between $\langle \Delta z^2 \rangle$ in HIT and quiescent fluid is smaller (with respect to what observed for $\langle \Delta x^2 \rangle$). In HIT, the diffusion coefficient for $\langle \Delta z^2 \rangle$ shows a maximum for $\phi = 1\%$, while it is minimum for $\phi = 10\%$ (as hindrance becomes more and more important with ϕ). In quiescent fluid, the diffusion coefficient is also found to decrease with ϕ. We have then investigated the particle-pair dynamics. We have found that the collision frequency, N_c, is larger in quiescent fluid than in HIT, for $\phi \leq 1\%$. Indeed, at these low concentrations drafting-kissing-tumbling events are frequent and the radial distribution function at contact is larger than in HIT (where mixing is more efficient). Instead, for $\phi \geq 5\%$ the collision frequency is larger in HIT than in quiescent fluid. Although the radial distribution function is similar (at contact, especially for $\phi = 10\%$), the normal relative velocity of approaching particles is substantially larger in HIT than in quiescent fluid, leading to the larger N_c. Interestingly, we also see that N_c appears to be almost proportional to the estimate obtained for small inertial particles uniformly distributed in space, though much smaller. The much smaller collision frequency found with respect to this estimate has been attributed to the strong slowing down of the particle approaching velocity at small separations, which is induced by viscous lubrication forces. The difference between N_c and the estimate decreases at larger ϕ, due to the larger probability of finding particle-pairs at contact.

Finally we have shown some statistics on the modulation of turbulence due to the settling particles. In particular, we find that the mean energy dissipation ϵ increases almost linearly with ϕ. On one hand, settling particles add energy to the system because of the gravitational force. On the other hand, particles add an important supplemental dissipative mechanism introduced by the no-slip condition at the particles surfaces. This leads to a clear reduction of Re_λ with ϕ. In addition, because the particle wakes are essentially oriented in the gravity direction, the anisotropy of the fluid velocity fluctuations increases with ϕ.

In the future, we are planning a dedicated study on the turbulence modulation in settling suspensions.

References

1. Aliseda, A., Cartellier, A., Hainaux, F., Lasheras, J.C.: Effect of preferential concentration on the settling velocity of heavy particles in homogeneous isotropic turbulence. J. Fluid Mech. **468**, 77–105 (2002)

2. Ardekani, M.N., Costa, P., Breugem, W.P., Brandt, L.: Numerical study of the sedimentation of spheroidal particles. International Journal of Multiphase Flow **87**, 16–34 (2016)
3. Bagchi, P., Balachandar, S.: Effect of turbulence on the drag and lift of a particle. Physics of Fluids (1994-present) **15**(11), 3496–3513 (2003)
4. Brenner, H.: The slow motion of a sphere through a viscous fluid towards a plane surface. Chemical Engineering Science **16**(3), 242–251 (1961)
5. Breugem, W.P.: A second-order accurate immersed boundary method for fully resolved simulations of particle-laden flows. J. Comput. Phys. **231**(13), 4469–4498 (2012)
6. Byron, M.L.: The rotation and translation of non-spherical particles in homogeneous isotropic turbulence. arXiv preprint arXiv:1506.00478 (2015)
7. Chrust, M.: Etude numérique de la chute libre d'objets axisymétriques dans un fluide newtonien. Ph.D. thesis, Strasbourg (2012)
8. Csanady, G.: Turbulent diffusion of heavy particles in the atmosphere. Journal of the Atmospheric Sciences **20**(3), 201–208 (1963)
9. Ern, P., Risso, F., Fabre, D., Magnaudet, J.: Wake-induced oscillatory paths of bodies freely rising or falling in fluids. Annual Review of Fluid Mechanics **44**, 97–121 (2012)
10. Feng, J., Hu, H.H., Joseph, D.D.: Direct simulation of initial value problems for the motion of solid bodies in a newtonian fluid part 1. sedimentation. Journal of Fluid Mechanics **261**, 95–134 (1994)
11. Fornari, W., Ardekani, M.N., Brandt, L.: Clustering and increased settling speed of oblate particles at finite reynolds number. Journal of Fluid Mechanics **848**, 696–721 (2018)
12. Fornari, W., Formenti, A., Picano, F., Brandt, L.: The effect of particle density in turbulent channel flow laden with finite size particles in semi-dilute conditions. Physics of Fluids (1994-present) **28**(3), 033,301 (2016)
13. Fornari, W., Picano, F., Brandt, L.: Sedimentation of finite-size spheres in quiescent and turbulent environments. J. Fluid Mech. **788**, 640–669 (2016)
14. Fornari, W., Picano, F., Sardina, G., Brandt, L.: Reduced particle settling speed in turbulence. Journal of Fluid Mechanics **808**, 153–167 (2016)
15. Fortes, A.F., Joseph, D.D., Lundgren, T.S.: Nonlinear mechanics of fluidization of beds of spherical particles. J. Fluid Mech. **177**, 467–483 (1987)
16. Garside, J., Al-Dibouni, M.R.: Velocity-voidage relationships for fluidization and sedimentation in solid-liquid systems. Industrial & engineering chemistry process design and development **16**(2), 206–214 (1977)
17. Good, G., Ireland, P., Bewley, G., Bodenschatz, E., Collins, L., Warhaft, Z.: Settling regimes of inertial particles in isotropic turbulence. J. Fluid Mech. **759**, R3 (2014)
18. Hampton, R., Mammoli, A., Graham, A., Tetlow, N., Altobelli, S.: Migration of particles undergoing pressure-driven flow in a circular conduit. Journal of Rheology **41**(3), 621–640 (1997)
19. Homann, H., Bec, J., Grauer, R.: Effect of turbulent fluctuations on the drag and lift forces on a towed sphere and its boundary layer. J. Fluid Mech. **721**, 155–179 (2013)
20. Huisman, S.G., Barois, T., Bourgoin, M., Chouippe, A., Doychev, T., Huck, P., Morales, C.E.B., Uhlmann, M., Volk, R.: Columnar structure formation of a dilute suspension of settling spherical particles in a quiescent fluid. Physical Review Fluids **1**(7), 074,204 (2016)
21. Jenny, M., Dušek, J., Bouchet, G.: Instabilities and transition of a sphere falling or ascending freely in a newtonian fluid. Journal of Fluid Mechanics **508**, 201–239 (2004)
22. Kawanisi, K., Shiozaki, R.: Turbulent effects on the settling velocity of suspended sediment. Journal of Hydraulic Engineering **134**(2), 261–266 (2008)
23. Lambert, R.A., Picano, F., Breugem, W.P., Brandt, L.: Active suspensions in thin films: nutrient uptake and swimmer motion. J. Fluid Mech. **733**, 528–557 (2013)
24. Lashgari, I., Picano, F., Breugem, W.P., Brandt, L.: Channel flow of rigid sphere suspensions: Particle dynamics in the inertial regime. International Journal of Multiphase Flow **78**, 12–24 (2016)
25. Maxey, M.: The gravitational settling of aerosol particles in homogeneous turbulence and random flow fields. J. Fluid Mech. **174**, 441–465 (1987)
26. Murray, S.P.: Settling velocities and vertical diffusion of particles in turbulent water. Journal of geophysical research **75**(9), 1647–1654 (1970)

27. Nielsen, P.: Turbulence effects on the settling of suspended particles. J. Sediment. Res. **63**(5) (1993)
28. Picano, F., Breugem, W.P., Brandt, L.: Turbulent channel flow of dense suspensions of neutrally buoyant spheres. J. Fluid Mech. **764**, 463–487 (2015)
29. Richardson, J., Zaki, W.: The sedimentation of a suspension of uniform spheres under conditions of viscous flow. Chemical Engineering Science **3**(2), 65–73 (1954)
30. Squires, K.D., Eaton, J.K.: Preferential concentration of particles by turbulence. Physics of Fluids A: Fluid Dynamics (1989-1993) **3**(5), 1169–1178 (1991)
31. Sundaram, S., Collins, L.R.: Collision statistics in an isotropic particle-laden turbulent suspension. part 1. direct numerical simulations. Journal of Fluid Mechanics **335**, 75–109 (1997)
32. Uhlmann, M., Doychev, T.: Sedimentation of a dilute suspension of rigid spheres at intermediate galileo numbers: the effect of clustering upon the particle motion. J. Fluid Mech. **752**, 310–348 (2014)
33. Vincent, A., Meneguzzi, M.: The spatial structure and statistical properties of homogeneous turbulence. J. Fluid Mech. **225**, 1–20 (1991)
34. Wang, L.P., Maxey, M.R.: Settling velocity and concentration distribution of heavy particles in homogeneous isotropic turbulence. J. Fluid Mech. **256**, 27–68 (1993)
35. Yang, T., Shy, S.: The settling velocity of heavy particles in an aqueous near-isotropic turbulence. Physics of Fluids (1994-present) **15**(4), 868–880 (2003)
36. Yang, T., Shy, S.: Two-way interaction between solid particles and homogeneous air turbulence: particle settling rate and turbulence modification measurements. J. Fluid Mech. **526**, 171–216 (2005)
37. Yeo, K., Dong, S., Climent, E., Maxey, M.R.: Modulation of homogeneous turbulence seeded with finite size bubbles or particles. International Journal of Multiphase Flow **36**(3), 221–233 (2010)
38. Yin, X., Koch, D.L.: Hindered settling velocity and microstructure in suspensions of solid spheres with moderate reynolds numbers. Phys Fluids **19**(9), 093,302 (2007)
39. Zaidi, A.A., Tsuji, T., Tanaka, T.: Direct numerical simulation of finite sized particles settling for high reynolds number and dilute suspension. International Journal of Heat and Fluid Flow **50**, 330–341 (2014)
40. Zhan, C., Sardina, G., Lushi, E., Brandt, L.: Accumulation of motile elongated microorganisms in turbulence. Journal of Fluid Mechanics **739**, 22–36 (2014)